CHEMICAL AND MORPHOLOGICAL CHANGES AT Al_2O_3/NiAl INTERFACES AND THEIR RELATIONSHIP TO SCALE ADHESION

P. Y. Hou
Lawrence Berkeley National Laboratory
Materials Sciences Division
MS: 62-203, 1 Cyclotron Rd., Berkeley, CA 94720

ABSTRACT

Ni-(40,50)at%Al alloys with different C and S contents were oxidized at 1000 -1150°C for various times in oxygen. Auger electron microscopy was used to study the interface chemistry after scale spallation in ultra high vacuum. The interfacial failure stresses were determined with a tensile pull tester and they were related to the interfacial pore density. Results show that sulfur did not segregate to the Al_2O_3/Ni50Al interface even after extended oxidation times. Small amounts, however, segregated to the Al_2O_3/Ni40Al interface. The difference in behavior may be related to the surface energy difference between Ni50Al and Ni40Al. On the interfacial void faces of Ni50Al, C first segregated, then it was replaced by S after longer oxidation times; the amount of segregants varied with different crystallographic orientation of the void face. On Ni40Al, S segregated much earlier on the void faces due to a faster diffusion rate in the Ni-rich NiAl. The apparent S diffusivity in Ni50Al and Ni40Al at 1000°C was determined to be 10^{-9} and 6×10^{-9} cm^2/s respectively. Excess sulfur in Ni40Al greatly increased the interfacial pore density. Preliminary results on interfacial failure stress showed that it decreased with increasing pore density, regardless of whether S was present at the interface, indicating that the major detrimental effect of S on scale adhesion may be to enhance interfacial pore formation.

INTRODUCTION

The segregation of indigenous sulfur impurity from an alloy to the Al_2O_3 scale/alloy interface during high temperature oxidation is often considered as the major cause that weakens the interface [1,2]. Systematic studies of the chemical changes at Al_2O_3/alloy interfaces have in recent years been carried out for FeCrAl [3], Fe_3Al and FeAl [4], where the alloys normally contain about 20 ppm of sulfur impurity. Although sulfur was found to be the major segregant at these scale/alloy interfaces, the segregation behavior, in terms of rate and amount, varied significantly with different alloys and differed from surface segregation. Whether similar behavior on FeAl can be expected for NiAl is unknown.

The oxidation behavior of NiAl has been studied extensively [5-11]. The first-formed oxide is θ or γ-Al_2O_3 that grows mainly by cation outward transport [9]. α-Al_2O_3 later nucleates at the scale/alloy interface [10] and the initially formed alumina also transforms to the more stable α form with time; growth of the α-Al_2O_3 is dominated by the transport of oxygen down alumina grain boundaries [9]. Because of this phase transformation, the oxidation kinetics shows two parabolic stages separated by a gradual transition. At 1000°C, the rate constant for the initial stage is about 10^{-12} g^2/cm^4s, and it is more than two orders of magnitude lower for the

later steady state [6]. Interfacial voids that are several times larger in diameter than the oxide grain sizes are often observed on the alloy surface [5,11]. These voids deepen into the alloy, often having facetted faces and distinct shapes that are associated with the alloy grains. Similar pore formation has been observed on FeAl alloys [12,13]. It was found that nucleation of these voids was the fastest during the initial stage of oxidation [12] where the scale grows predominantly by cation outward transport. Sulfur in the alloy has been suggested to enhance pore formation by lowering its surface energy [14]. Surface impurities can also have the same effect [15].

Despite these prior studies, the chemistry of the Al_2O_3/NiAl interfaces has never been examined. The purpose of this work is to study the chemical changes at Al_2O_3/NiAl interfaces as oxidation proceeds, and relates that to the interface morphology and the interfacial strength. This paper summarizes initial results on these studies performed on several different NiAl alloys with different purity.

EXPERIMENTAL

Different Ni-50at%Al (NiAl) and Ni-40at%Al alloys were used in this study, all of them made with high purity starting materials. Their compositions and some impurity contents are given in Table 1. Three batches of NiAl and one Ni-40at%Al alloy were obtained from Oak Ridge National Laboratory. They were prepared by induction melting, followed by annealing at 1300°C for 4 hours. The labels (1)-(3) for the NiAl alloys are used to rank their purity in terms of S and C contents, where (1) is the purest. One of the Ni-40Al and the S-doped Ni-40Al alloys were made at LBNL by arc melting, followed by annealing at 1150°C for 15 hours. All the normal purity alloys contain small amounts of sulfur impurity, about 2-6 ppma. The S-doped alloy was made by co-melting with NiS, and it contains more than 30 ppm of sulfur. The oxidation and segregation behaviors of the three NiAl alloys and the two Ni40Al alloys are often similar, so unless otherwise noted, the results presented here do not make distinctions between the different batches.

Table 1: Chemical Analysis of NiAl Alloys by Combustion or GDMS (denoted by *) Analysis

Alloy	Concentration (at%)		Concentration (ppma)				
	Ni	**Al**	**S***	**C**	**Cl**	**P**	**B**
NiAl (1)	50.7	49.3	3.5	320	<0.01*	2.8*	43.8*
NiAl (2)	49.91	50.05	3.7	360			40
NiAl (3)	49.74	50.19	4.3	710			
Ni-40Al	59.7	40.3	6.6	380			30
Ni-40Al[+]	60.1	39.8	2.2	150			
Ni-40Al (S-doped)[+]	60.9	40.0	34.7	420			

[+]Alloys made at LBL. Others were made at ORNL.

Specimen discs about 1-2 cm in diameter and 1 mm thick were cut from the ingot. All sides of the specimens were grounded using SiC paper with one main face polished to a 1 μm surface finish with diamond paste and the specimen was cleaned ultrasonically in acetone before oxidation in flowing, dry oxygen. Most oxidation tests were performed at 1000°C, with a few at 1100 and 1150°C, in a horizontal furnace, where the specimen was placed in an alumina boat with a thermocouple at its back. After the desired oxidation time, which varied from 10 min to 100 hours, the boat and specimen were quickly pulled out of the furnace and cooled in ambient air. A Cahn TGA system was used for thermogravemetic analysis at 1000°C; both faces of these specimens were polished to the 1 μm finish.

Structure of the scale was studied using X-ray diffraction and the morphology examined using scanning electron microscopy (SEM). Chemistry of the scale/alloy interface was studied using Auger electron spectroscopy (AES) after the scale was removed in the ultra high vacuum (UHV) chamber of the AES by the forces of a scratch made on the specimen surface [16]. This technique caused spalling of the scale adjacent to the scratch, exposing areas of the underlying alloy surface that can be examined using a 0.5-1 μm size Auger probe. The underside of the oxide was also studied on scale pieces that flipped over during the spalling process, so both sides of the interface, although from different locations, can be examined. Images from secondary electrons were used to distinguish features at the alloy surfaces. These usually include facetted voids and smooth or α-Al_2O_3 imprinted interface areas. Several different areas covering more than one alloy grains were often examined. Surveys were performed on many similar features in order to attain a statistical analysis of the results.

The strength of the scale/alloy interface was studied using a Quad Group Sebastian 5 pull-tester, where a 3 mm diameter stub with a thin film of adhesive was secured onto the oxidized surface, and then the stub was pulled at an inverted position (Fig. 1a) with a constant loading rate until failure. If the failure took place at the scale/alloy interface and if the entire area failed, an example shown in Fig. 1b, the data

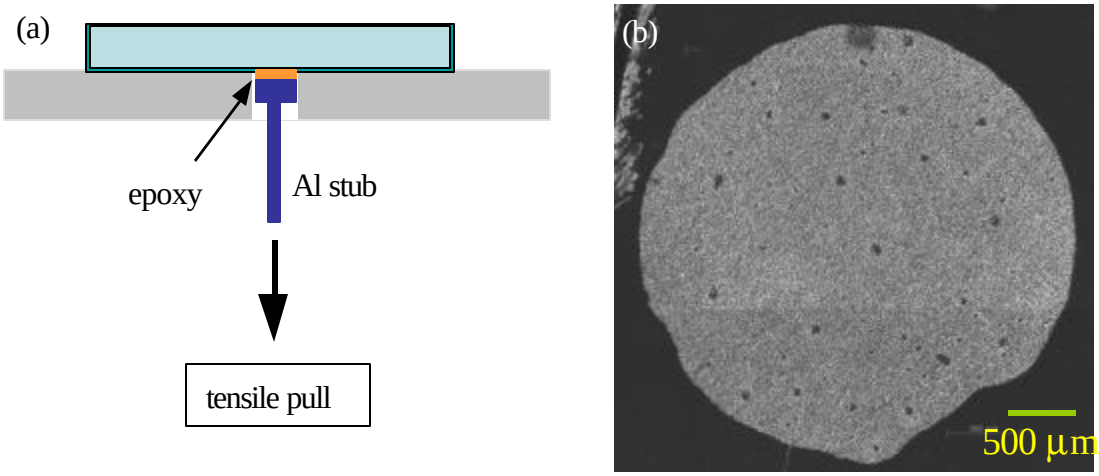

Figure 1: (a) Schematics of the pull test setup, (b) example of a failed area on Ni40Al after oxidation at 1000°C for 26h.

was used with the failure load divided by the stub area to provide a value of the interface strength. The adhesive was cured at 150°C and has a maximum strength of 103 MPa. Several stubs were tested on each specimen, and then every failed area was examined under the SEM. Micrographs of randomly selected regions were taken to calculate the number of interfacial pores on each area. Since the specimens being compared were oxidized for the same time at the same temperature, i.e., 26 hours at 1000°C, the pore size was not taken into consideration.

RESULTS

Specimen weight gain as a function of time was examined for all the alloys at 1000°C up to 50 hours. All results showed a fast initial stage followed by a slower steady state; the rates of both stages obeyed parabolic kinetics and the rate constants for the two stages are in the range of $(2\text{-}6)\text{x}10^{-12}$ and $(2\text{-}5)\text{x}10^{-14}$ g^2/cm^4s respectively. These numbers agree well with those reported earlier by others for NiAl [8]. Initially, very fined-grained θ-Al_2O_3 formed on both NiAl and Ni40Al, leaving a rather featureless interface, as seen in Fig. 2a. α-Al_2O_3 later nucleated at the scale/alloy interface, giving rise to interfaces that clearly comprised of Al_2O_3 grain imprints, examples are seen in Fig. 2b for NiAl and Fig. 5a for Ni40Al.

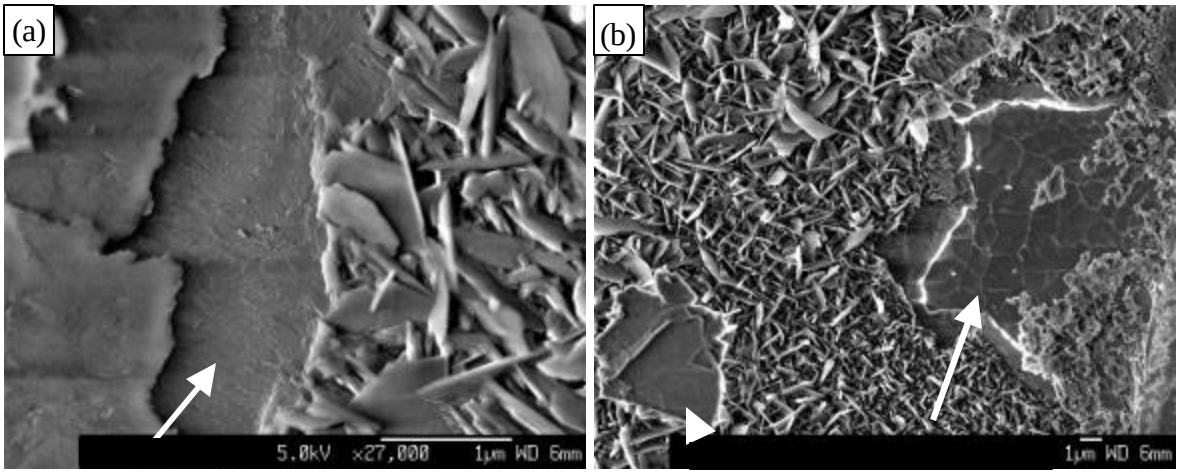

Figure 2: SEM micrographs of typical scale morphology on NiAl showing (a) initial transition alumina and smooth alloy surface after 5hr at 1000°C and (b) α-Al_2O_3 that had nucleated at the scale/alloy interface and the imprinted alloy surface after 65 hr.

No impurities were detected on the oxide side of the interface; only O and Al were observed. All impurities, if present at the interface, remained on the alloy side after scale spallation, where voids that deepened into the alloy were often present. These voids are strongly facetted and their shapes dictated by the alloy grain orientation (Fig. 3). On the NiAl, carbon segregated to the pore surfaces initially and this segregation was strongly orientation dependent. The pore faces seen on Fig. 3, for example, were either free from any impurity or contain a high concentration of carbon, as seen by the AES spectra in Fig. 4 and the surface concentrations summarized in Table 2, where these were calculated using tabulated sensitivity factors [17]. The carbon content on all analyzed void faces can

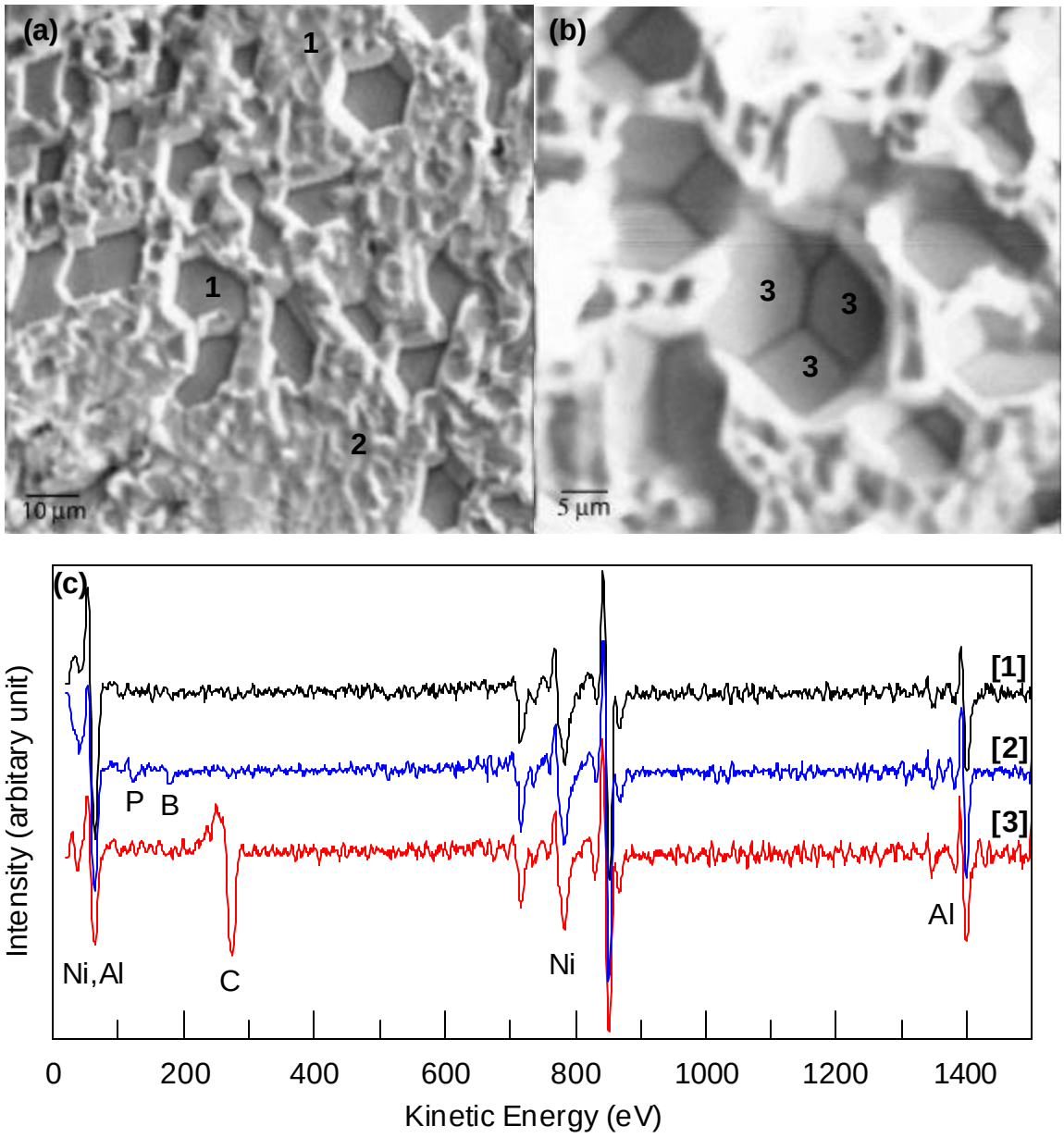

Figure 3: (a), (b) SEM micrographs of two groups of voids found on two different NiAl(3) alloy grains after oxidation at 1000°C for 26 hours. (c) AES spectra of points indicated on the micrographs. All the void faces on (a) are of composition [1]. About 50% of the analyzed interface areas had the composition [1] while the rest are that of [2]. All the void faces in Fig. 3(b) had the composition [3].

be grouped into three values. The first lies within a high background level due to C surface contamination even in the UHV. Within experimental error, S was not detected on the void surface after 26 hrs at 1000°C. The interface areas on the NiAl were mostly free from any impurities, other than an occasional presence of B and also some P. The B peak appeared near 180 eV, which could also be identified as Cl. However, since these alloys have higher concentrations of B impurity than Cl, and B, not Cl, had been found to segregate to NiAl grain boundaries [18], this peak was therefore identified as B. With longer oxidation times on the NiAl, S replaced the C on some void faces while others continued to be covered with C. The

interface, however, remained free from S or C, except with some occasional B and P, as shown in Fig. 4 and Table 2. At higher temperatures, S covered more void faces and its coverage was also orientation dependent, yet the interface areas continued to be free from S and C.

Table 2: Summary of C and S concentration (in at%) on different Al_2O_3/NiAl interfaces

oxidation condition	NiAl				Ni-40Al			
	Interface		Voids		Interface		Voids	
	C	S	C	S	C	S	C	S
1000°C 10m					0	0.7±0.3	0	7.7±0.4
30m					0	0.9±1.2	0	5.6±1.4
1h					0	1.8±0.8	0	9.0±1.3
2h	0.6±1.3	0						
5h	3.2±2.2	0						
26h	2.8±1.5	0	4.0±4.9 28.4±2.9 41.0±4.6	0.1±0.3 0 0	4.2±3.0	1.4±0.9	3.3±2.5	8.0±0.6
65h	0	0						
100h	1.4±2.4	0	2.4±2.8 19.6±6.6 33.0±5.0	2.8±1.2 1.3±1.2 0				
1100°C 100h	3.4±2.4	0.2±0.2						
1150°C 100h	0.7±1.6	0.1±0.2	0.3±0.7 11.7±4.8 48.3±10.5	4.5±2.4 2.9±2.6 0.2±0.3				

Shaded areas are data obtained from the S-doped Ni40Al specimens.

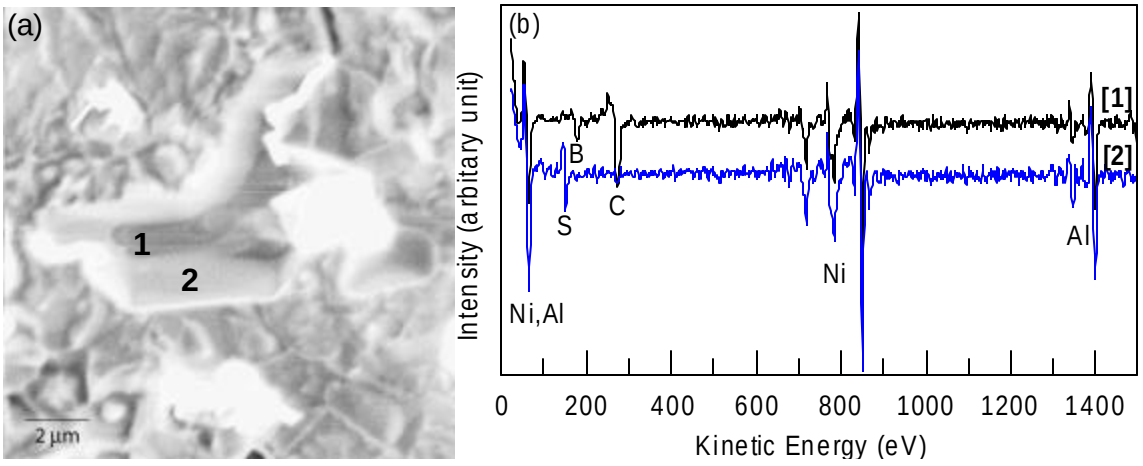

Figure 4: NiAl(2) interface after 100 hrs at 1000°C. (a) SEM image of the analyzed area, (b) AES surveys of points 1 and 2 on (a) showing S replacing C on some void faces.

The interface microstructure found on the Ni-40Al was similar to that of the NiAl, an example is given in Fig. 5a, showing α-Al_2O_3 imprinted interface and facetted interfacial voids on the alloy surface under the spalled scale. The segregation behavior of Ni-40Al compared with that of the NiAl was different in two ways. First, in spite of similar amounts of S and C impurities in the alloy, S was found to segregate to the void faces after the same oxidation time at the same temperature, i.e., 26h at 1000°C (Table 2). Quantitative analysis of the sulfur content also showed that it was significantly higher than that found on the NiAl voids. The amount is similar to that found on the voids formed on Fe-40at%Al [12], where the excess over the saturation level of half a monolayer was determined to be the result of S co-segregation with Al. The same mechanism is believed to be responsible for the excess S observed here on the Ni40Al. Work is in progress to obtain better Al concentration of the starting alloys to determine the degree of Al enrichment on all void faces. Carbon was not found to segregate at the void surface or at the interface. Unlike NiAl, where the interface is always free from S and C, these interfaces contained a small amount of S. Typical AES spectra for the interface and the void faces of the Ni40Al are given in Fig. 6.

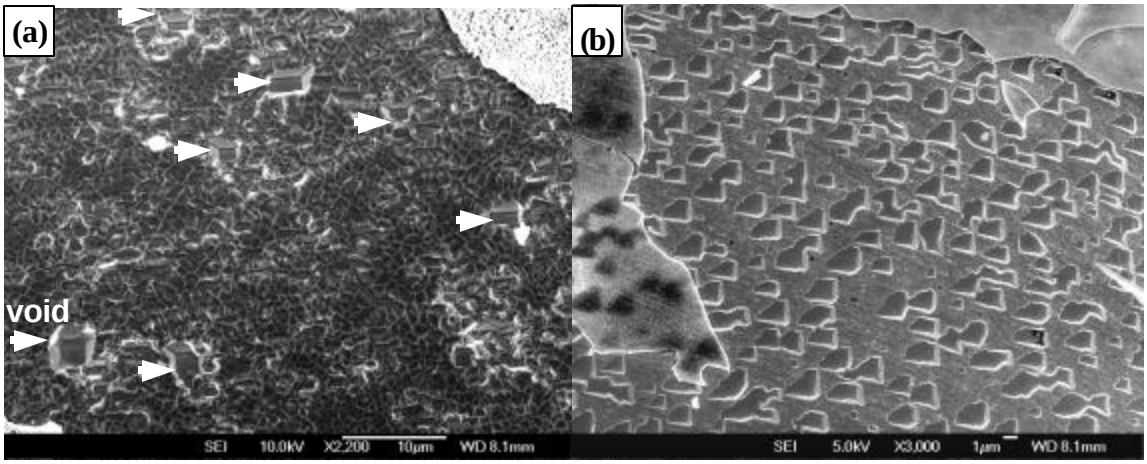

Figure 5: Interface morphology of (a) Ni-40Al, 1000°C, 26 hr and (b) S-doped Ni-40Al, 1000°C, 10 min.

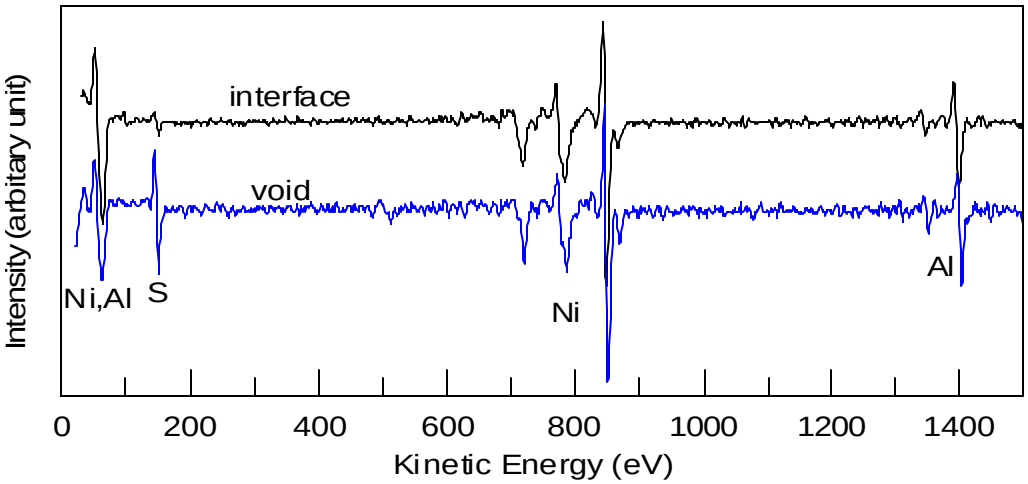

Figure 6: AES spectra of typical interface and void surface on all Ni-40Al alloys.

The S-doped Ni-40Al, containing >30 ppm S, had similar interface chemistry as the normal purity Ni-40Al that contains only a few ppm of S. However, scale adhesion on the S-doped specimens was extremely poor. After 26 hr oxidation, almost the entire scale spalled upon cooling, so only specimens with thin scales that formed for short times could be analyzed. The most pronounced effect of the S-doping was to increase the number of pores at the scale/alloy interface, as seen in Fig. 5b.

The relationship between interfacial failure stress and pore density are shown in Fig. 7 for scales oxidized at 1000°C for 26 hours, except for the S-doped one where oxidation was only carried out for 10 minutes. Five groups of data points are seen that

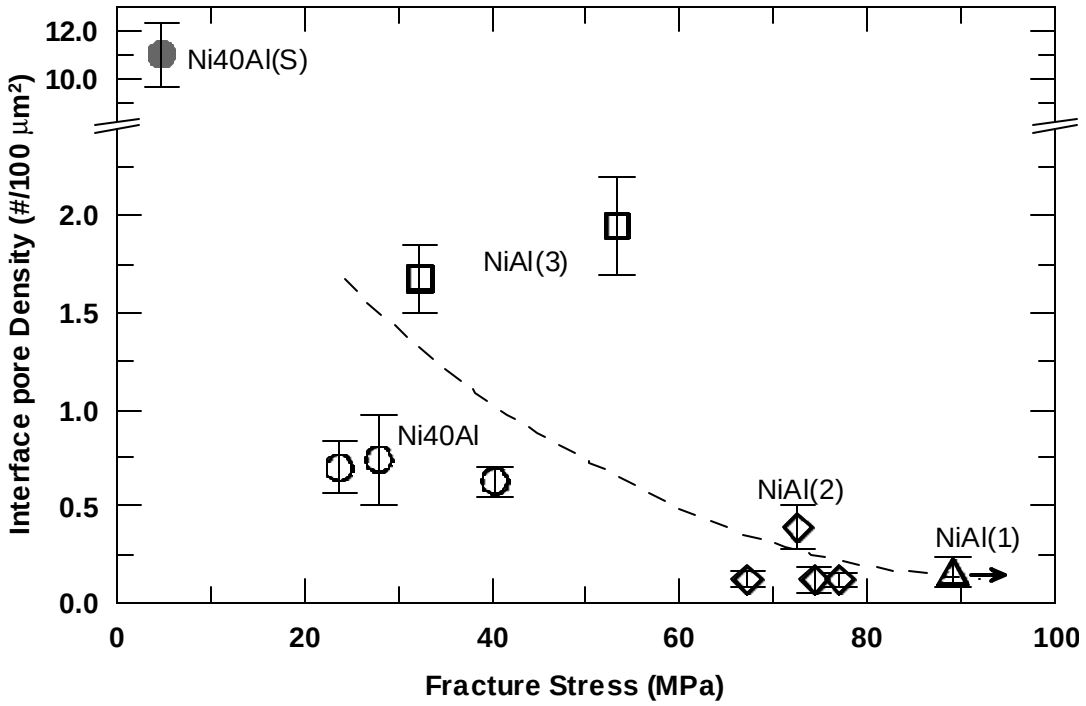

Figure 7: Relationship between interfacial failure stress and interface pore density, after oxidation at 1000°C for 26 hr (but only 10 min for the S-doped sample).

belong to five different alloys. The oxide scale on the purest batch of NiAl was difficult to fail. Only one out of three tested stubs showed partial failure at the scale/alloy interface, so the true failure stress should be higher than that indicated by the data point, hence an arrow was drawn pointing to higher stress levels. The high pore density on the NiAl(3) alloy may be a result of its lowest purity of the three NiAl alloys, with slightly higher S content and greater C content. However, these data were mistakenly obtained from the backside of the specimen that had a rougher surface finish, which has been shown to cause more pore formation [15]. While all the normal purity specimens were oxidized for the same time to produce similar scale thickness, the scale on the 10 min S-doped specimen was much thinner; therefore, it does not provide a direct comparison with the rest of the data, because scale thickness can affect the failure stress. Preliminary experiences showed that thinner scales gave rise to higher failure stresses. However, these data together still show a clear relationship between interface pore density and interfacial strength. The higher strength shown by NiAl(3) relative to the trend line may be due

to its rougher surface that made crack propagation more difficult. On the other hand, the lower strength of the Ni40Al may be due to the small amount of S present at the interface between the voids, making crack propagation easier. Work is currently underway to obtain more data from different specimens to better relate the failure stress to interface microstructures.

DISCUSSIONS

Impurity segregation to Al_2O_3/NiAl and Al_2O_3/Ni40Al interfaces, or even to interfacial void surfaces on NiAl and Ni40Al, has been shown to be quite different. To the void surfaces, which are the same as free surfaces under extremely low oxygen partial pressures, sulfur segregated strongly to normal purity Ni40Al after 26 hrs at 1000°C, but under the same condition, only carbon was observed on NiAl. After longer oxidation time or higher temperatures, S began to segregate and replaced the carbon. These apparent different rates of sulfur segregation to the void faces between NiAl and Ni40Al suggest that the diffusion of S in Ni50Al is slower than in Ni40Al, given that the two starting alloys have similar sulfur contents, between 2-6 ppm. Using the model of Lea and Seah [19], diffusion coefficients of S in the two alloys are calculated to be about 6×10^{-9} cm^2/s for Ni40Al and 1×10^{-9} cm^2/s for NiAl. Diffusion of Ni in NiAl has been shown to be very sensitive to stoichiometry [20] due to strong variations of defect concentrations with composition. At 1300K, D_{Ni} increases from 10^{-12} to 10^{-11} cm^2/s from stoichiometric NiAl to Ni-40at%Al. These values are 10^3 times lower than the D_S calculated from the segregation results reported here. However, this difference agrees with recent data from S segregation studies on NiAl surfaces [21], which determined that S diffusion in NiAl is about 3 orders of magnitude faster than Ni at 800°C.

The amount of segregated C or S on the NiAl void surfaces was very dependent on the crystallographic orientation of the void face. The amount of S never exceeded its saturation level, which is about 0.5 monolayer [21]. However, on some faces, high concentrations of carbon exceeding a monolayer were detected. These kinds of behavior have been seen on Ni surfaces. Blakely and co-workers [22,23], for example, have found that C segregates to the (100) and (110) faces of Ni, but not to the (110) face. Furthermore, the amount of segregated carbon was found to vary with temperature [22]. At >907°C, only a dilute coverage was found; between about 800-900°C, a graphitic monolayer exits and below ~800°C, multiplayer epitaxial graphite precipitates formed on the Ni surface. If similar temperature dependence is obeyed on the NiAl surface, the high concentrations of C found in this study must have segregated during cooling. Void faces with very high C concentrations were sometimes found close to internal carbide particles. Work is in progress to determine the orientation of different void faces using electron backscatter diffraction (EBSD), in order to correlate the segregation behavior to the crystallographic orientations.

The difference between Al_2O_3/NiAl and Al_2O_3/Ni40Al interfaces is that the latter contained a small amount of S (less than 2 at%), but the former was either clean within the delectability of AES, or contained small amounts of B and P. The presence of S on the Ni40Al probably prevented B and P segregation, as segregants often compete for sites. The amount of S found on the Ni40Al interface was significantly lower than that found on FeCrAl where S co-segregates with Cr [3]; it is also about 50% less than that found on Fe40Al [24] for reasons yet

unknown. Why S segregates to the Ni40Al but not to the Ni50Al interface is also not clear. The difference should not be due to the minor difference in bulk S content. The oxide formation process and the oxidation rate for both types of alloys are also very similar. It is therefore unlikely that the oxide above the two alloys would dictate the interface property in any way as to affect the interfacial segregation behavior. A more probable explanation lies in the stability of the two NiAl surfaces. The ordered NiAl has lower energies than the Ni40Al [25], so segregation of S would be more favored on Ni40Al to lower its energy. There is also indirect evidence from wetting studies of NiAl on sapphire showing that the interface energy increases with decreasing Al content in the NiAl [26].

The pull test used in this study is a technique that lacks a well-defined pre-crack so that failure depends on internal defects. Since failure took place at the scale/alloy interface and interfacial pore diameters are often as large as the scale thickness, about 1-2 μm, these pores are therefore the most likely internal defects. Alloy grain boundaries may be an additional defect source, especially if grain boundary grooving occurred during oxidation. However, preliminary analysis did not show a relationship between the total boundaries length on a failed area and its failure stress. Although data are limited, the results shown in Fig. 7 indicate a clear relationship between the pore density at the interface and the interface strength, which is not surprising. What is interesting is that the major effect of sulfur on scale adhesion is seen to increase interfacial pore density, where S lowers the activation energy for pore nucleation by reducing the alloy surface energy [15]. The presence of S at the interface may have an additional effect on interfacial fracture toughness, but this seems secondary compare to its strong influence on enhancing pore formation.

CONCLUSIONS

1. Small amounts of S segregate to Ni40Al interfaces, but none to Ni50Al interfaces, probably due to the lower surface energy of the Ni50Al. B and P were found on some areas of the otherwise clean Ni50Al interfaces.

2. C segregates to interfacial voids, but not to interfaces. With time, S replaces C on void faces. The S diffusion rate in Ni40Al is about 6 times faster than in Ni50Al. Segregation of S and C on the Ni50Al void faces is strongly orientation dependent.

3. Interface strength is dictated by interfacial pore density. The major role of sulfur impurity in the NiAl alloy is to enhance this pore formation. The presence of S at the interface may only have a secondary effect on accelerating crack propagation.

ACKNOWLEDGMENT

The author would like to thank Dr. Bruce Pint of ORNL for supplying some of the alloys, and to Mr. Christopher Van Lienden for his assistance with the pull test and the interfacial pore density analysis. This research is sponsored by the U. S. Department of Energy under contract No. DE-AC03-76SF00098.

REFERENCES

1. A. W. Funkenbusch, J. G. Smeggil, and N. S. Bornstein, *Metall. Trans. A*, **16A**, 1164 (1985).
2. J. L. Smialek, *Metall. Trans.* **22A**, 739 (1991).
3. P. Y. Hou, *Mater. and Corr.*, **51**, 329 (2000).
4. P. Y. Hou, *Mater. Sci. Forum*, **369-372**, 23 (2001).
5. R. Hutchings, M. H. Loretto and R. E. Smallman, *Metal Science*, **15**, 7 (1981).
6. J. Doychak and M. Rühle, *Oxid. Met.*, **31**, 431 (1989).
7. B. A. Pint, *Oxid. Met.*, **49**, 531 (1998).
8. M. W. Brumm and H. J. Grabke, *Corr. Sci.*, **33,** 1677 (1992).
9. E. Schumann J. C. Yang, M. J. Graham and M. Rühle, *Mater. Corros.*, **46**, 218 (1995).
10. J. C. Yang, K. Nadarzinski, E. Schumann and M. Rühle, *Scripta Met*, **33**, 1043 (1995).
11. M. W. Brumm, H. J. Grabke, *Corr. Sci.*, **34**, 547 (1993).
12. P. Y. Hou, Y. Niu and C. Van Lienden, *Oxid. Met.*, **59**, 41 (2003).
13. C. H. Xu, W. Gao and H. Gong, *High Temp. Mater. and Proc.*, **19**, 371 (2000).
14. H. J. Grabke, D. Wiemer and H. Viefhaus, *Appl. Surf. Sci.*, **47**, 243 (1991).
15. P. Y. Hou and C. Van Lienden, presented at Microscopy of Oxidation 5, Limerick, Ireland, Aug. 26-28, 2002, accepted for publication in *Mater. at High Temp.*
16. P. Y. Hou, in *"High Temperature Corrosion and Materials Chemistry"*, ed. P. Y. Hou, M. J. McNallan, R. Oltra, E. J. Opila and D. A. Shores, pp. 198-210, the Electrochem. Soc., 1998.
17. Davis, N. C. MacDonald, P. W. Palmberg, G. E. Riach and R. E. Weber, *Hand Book of Auger Electron Spectroscopy*", 2nd edition, Physical Electronic Indus. Inc., 1978.
18. R. Jayaram and M. K. Miller, *Acta mater.*, **42**, 1561 (1994).
19. C. Lea and M. P. Seah, *Philo. Mag.*, **35**, 213 (1977).
20. St. Frank, S. V. Divinski, U. Sodervall and Chr. Herzig, *Acta mater.*, **49**, 1399 (2001).
21. L. Rivoaland, V. Maurice, M.-P. Bacos and P. Marcus, *Surf. Inter. Ana.*, **34**, 400 (2002).
22. J. C. Shelton, H. R. Patil and J. M. Blakely, *Surf. Sci.*, **43**, 493 (1974).
23. L. C. Isett and J. M. Blakely, *Surf. Sci.*, **58**, 397 (1976).
24. P. Y. Hou and John Moskito, *Oxid. Met.*, **59**, 559-574 (2003).
25. G. D. Ayushina, E. S. Levin, P. V. Del'd, *Russ J. Phys. Chem*. **43**, 2756 (1969).
26. E. Saiz, R. M. Cannon and A. P. Tomsia, *Acta mater.*, **48**, 4449 (2000).